iScience

CellPress
OPEN ACCESS

Article

Airway epithelial cells and macrophages trigger IL-6-CD95/CD95L axis and mediate initial immunopathology of COVID-19

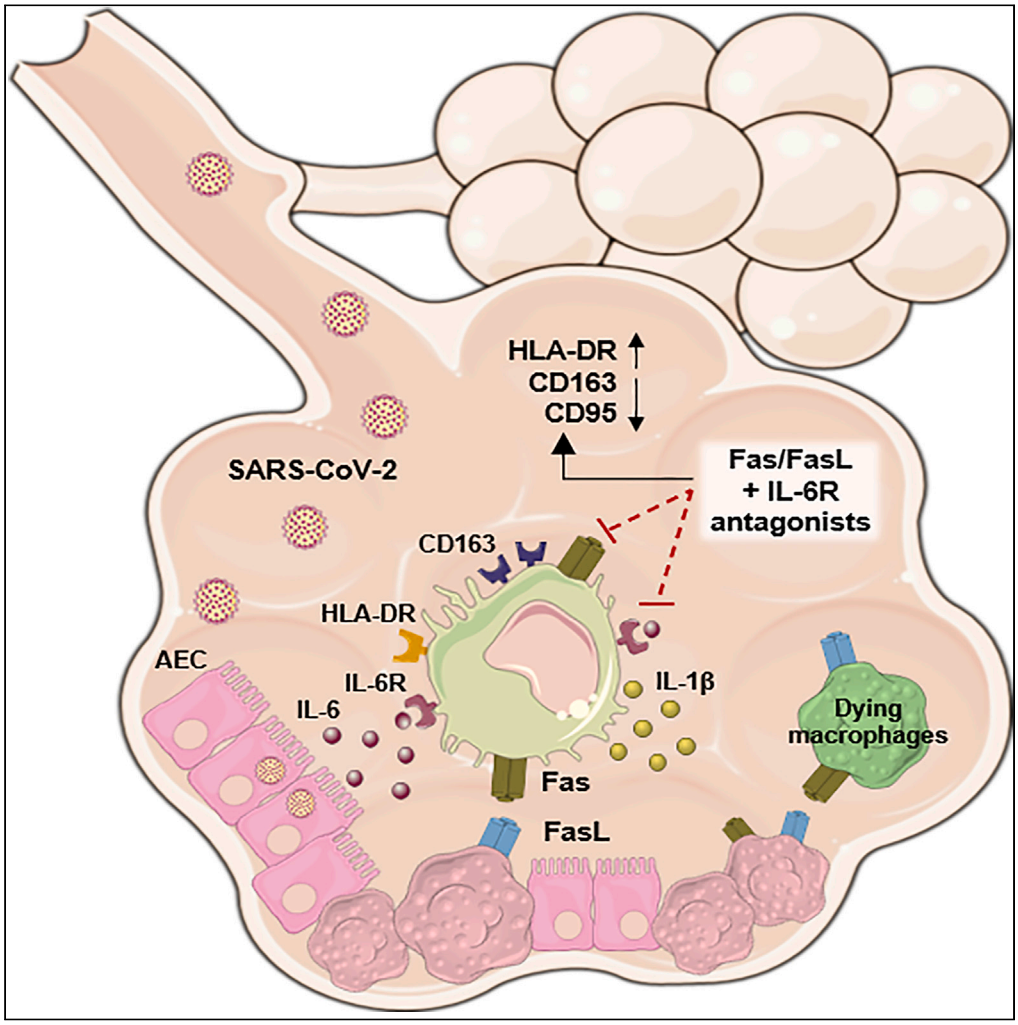

Thais F.C. Fraga-Silva, Ualter G. Cipriano, Marcilio J. Fumagalli, ..., Maria Auxiliadora-Martins, Rita C. Tostes, Vania L.D. Bonato

vlbonato@fmrp.usp.br

Highlights

SARS-CoV-2-infected airway epithelial cells (AEC) secrete IL-6 and express FasL

Infected apoptotic AEC or IL-6 increases Fas and CD163 expression on macrophages

Fas/FasL or IL-6 receptor antagonists prevent macrophage dysfunction

Non-canonical CD95L-CD95 pathway drives macrophage activation and dysfunction

Fraga-Silva et al., iScience *26*, 108366
December 15, 2023
https://doi.org/10.1016/j.isci.2023.108366

iScience

CellPress
OPEN ACCESS

Article

Airway epithelial cells and macrophages trigger IL-6-CD95/CD95L axis and mediate initial immunopathology of COVID-19

Thais F.C. Fraga-Silva,[1] Ualter G. Cipriano,[2] Marcilio J. Fumagalli,[2] Giseli F. Correa,[2] Carlos A. Fuzo,[3] Douglas dos-Santos,[4] Fabiola L.A.C. Mestriner,[5] Christiane Becari,[5] Andrea Teixeira-Carvalho,[6] Jordana Coelho-dos-Reis,[7] Mayra G. Menegueti,[8] Luiz T.M. Figueiredo,[2,9] Larissa Dias Cunha,[4] Olindo A. Martins-Filho,[6] Marcelo Dias-Baruffi,[3] Maria Auxiliadora-Martins,[5] Rita C. Tostes,[10] and Vania L.D. Bonato[1,2,11,*]

SUMMARY

Airway epithelial cells (AEC) infected with SARS-CoV-2 may drive the dysfunction of macrophages during COVID-19. We hypothesized that the direct interaction of AEC with macrophages mediated by CD95/CD95L or indirect interaction mediated by IL-6 signaling are key steps for the COVID-19 severe acute inflammation. The interaction of macrophages with apoptotic and infected AEC increased CD95 and CD163 expression, and induced macrophage death. Macrophages exposed to tracheal aspirate with high IL-6 levels from intubated patients with COVID-19 or to recombinant human IL-6 exhibited decreased HLA-DR expression, increased CD95 and CD163 expression and IL-1β production. IL-6 effects on macrophages were prevented by both CD95/CD95L antagonist and by IL-6 receptor antagonist and IL-6 or CD95 deficient mice showed significant reduction of acute pulmonary inflammation post-infection. Our findings show a non-canonical CD95L-CD95 pathway that simultaneously drives both macrophage activation and dysfunction and point to CD95/CD95L axis as therapeutic target.

INTRODUCTION

SARS-CoV-2 (severe acute respiratory syndrome coronavirus 2), the causative agent of coronavirus disease 2019 (COVID-19), primarily infects epithelial cells in the respiratory tract. The Spike protein on the virus surface is recognized by the angiotensin-converting enzyme 2 (ACE2), which is highly expressed by epithelial cells of the higher airways, as nasopharynx, and lower airways, as alveolar epithelial cells, particularly by type II pneumocytes.[1–4] Viral particles were identified within bronchial epithelial cells, alveolar type I and II cells.[4] The infection of airway epithelial cells (AEC) disrupts intercellular junctions and the contact of AEC with the basement membrane.[5,6] SARS-CoV-2 infection of human AEC *in vitro* induces a cytopathic effect,[6] stimulating caspase-8-dependent IL-1β production,[7] activating gene expression of inflammatory factors, and inhibiting type-I IFN production.[8]

Patients with severe and critical forms of COVID-19 exhibit increased serum concentrations of IL-6 and IL-10, lower expression of HLA-DR on monocytes, and increased neutrophil to lymphocyte ratio in the peripheral blood.[9,10] Moreover, severe patients with COVID-19 are grouped in 2 immunotypes: 1- deceased patients that remained a short time at the hospital, exhibited high viral load and low diffuse alveolar damage (DAD); 2- deceased patients that remained a long time at the hospital, had lower viral load and significant DAD and immunopathology compared to the group 1.[11,12] These findings show that the dysregulation of the immune response and immunopathology are hallmarks of severe COVID-19 and that the severe pulmonary disease is heterogeneous and have distinct immunotypes.

[1]Department of Biochemistry and Immunology, Ribeirao Preto Medical School, University of Sao Paulo, Ribeirao Preto, Sao Paulo 14049-900, Brazil
[2]Basic and Applied Immunology Program, Ribeirao Preto Medical School, University of Sao Paulo, Ribeirao Preto, Sao Paulo 14049-900, Brazil
[3]Department of Clinical Analysis, Toxicology and Food Sciences, School of Pharmaceutical Sciences of Ribeirão Preto, University of Sao Paulo, Ribeirao Preto, Sao Paulo 14049-900, Brazil
[4]Department of Cell Biology, Ribeirao Preto Medical School, University of Sao Paulo, Ribeirao Preto, Sao Paulo 14049-900, Brazil
[5]Department of Surgery and Anatomy, Ribeirao Preto Medical School, University of Sao Paulo, Ribeirao Preto, Sao Paulo 14049-900, Brazil
[6]René Rachou Institute, Oswaldo Cruz Foundation, FIOCRUZ-Minas, Belo Horizonte, Minas Gerais 30190-009, Brazil
[7]Department of Microbiology, Biological Science Institute, Federal University of Minas Gerais, Belo Horizonte, Minas Gerais 31270-901, Brazil
[8]Department of General and Specialized Nursing, Ribeirao Preto Nurse School, University of Sao Paulo, Ribeirao Preto, Sao Paulo 14049-900, Brazil
[9]Virology Research Center, Ribeirao Preto Medical School, University of Sao Paulo, Ribeirao Preto, Sao Paulo 14049-900, Brazil
[10]Department of Pharmacology, Ribeirao Preto Medical School, University of Sao Paulo, Ribeirao Preto, Sao Paulo 14049-900, Brazil
[11]Lead contact
*Correspondence: vlbonato@fmrp.usp.br
https://doi.org/10.1016/j.isci.2023.108366

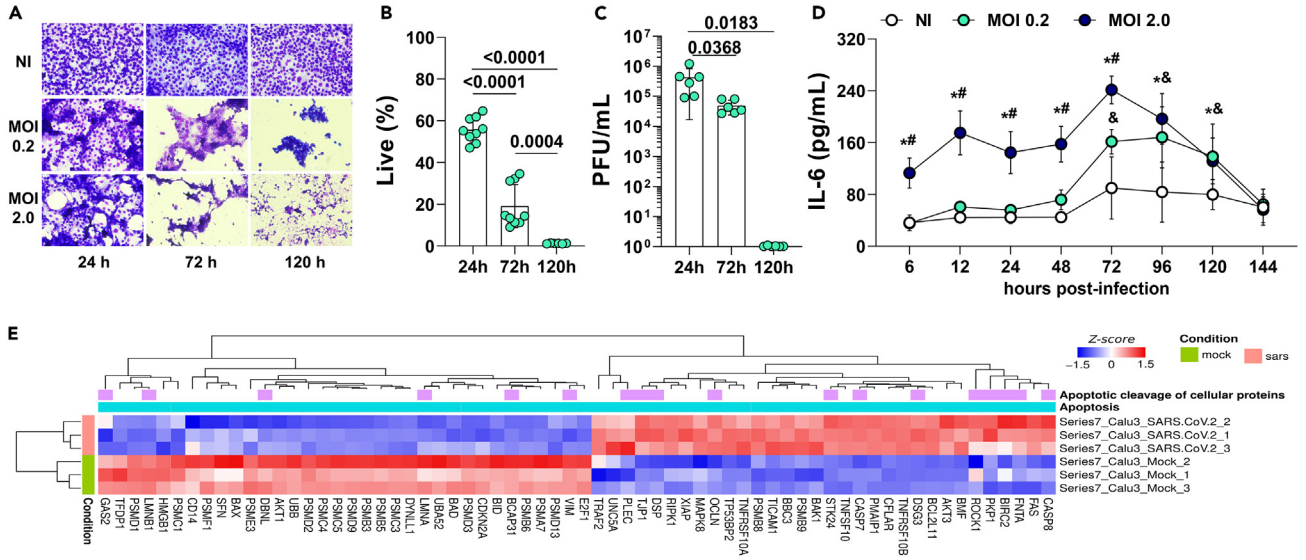

Figure 1. SARS-CoV-2 induces death and IL-6 secretion in airway epithelial cells

(A and B) Calu-3 cells were infected with SARS-CoV-2 at the multiplicity of infection (MOI) 0.2 and 2.0. Cytopathic effect was evaluated using (A) Panotic staining and (B) flow cytometric analysis of live cells (annexin V^-FVS^-).

(C) Viral load was measured by plaque-forming units (PFU/mL) using the supernatants of Calu-3-infected cells at 24, 72 and 120 h post-infection (p.i.).

(D) IL-6 concentration was measured in the supernatants derived from non-infected (NI) and SARS2-infected cells at 6 to 144 h p.i.

(E) Normalized expression (*Z* score) of differentially expressed genes related to apoptosis pathways in infected and non-infected (mock) cells. Data represent the mean ± SD of at least two independent experiments performed in triplicate. (D) *p < 0.05, MOI 2.0 vs. NI; #p < 0.05, MOI 2.0 vs. MOI 0.2, and & p < 0.05, MOI 0.2 vs. NI. Bars depict the exact p values.

Postmortem examination revealed a predominance of myeloid cells, mostly macrophages, along with $CD4^+$ and $CD8^+$ T cells infiltration in the pulmonary parenchyma of patients with COVID-19,[13] indicating a critical role for macrophages in the immunopathology and in the dysregulation of the immune response in the lungs.[14] Although it has been shown that SARS-CoV-2 infects AEC, induces cell death, DAD, cytokine secretion, acute inflammation, neutrophil influx, and neutrophil extracellular traps (NET),[15] the initial mechanisms that drive the interactions of lung epithelial cells and macrophages and how these early events contribute to the dysregulated immune response induced by macrophages in the lungs are unknown.

CD95L-CD95 signaling induces canonical lymphocyte death in COVID-19.[16,17] However, whether the CD95L-CD95 axis leads to macrophage activation and dysfunction in COVID-19 remains to be investigated. Severe patients with COVID-19 exhibit higher CD163 expression in lungs macrophages[18–20] and lower HLA-DR in monocytes.[9,21,22] In addition, lung monocytes and macrophages from patients with severe COVID-19 show compromised efferocytosis, i.e., the engulfment of apoptotic cells.[23] We hypothesized that CD95L-CD95 signaling and IL-6 secretion drive AEC death and activation of inflammatory responses by macrophages. To investigate the activation of very early events of the innate response leading to hyperinflammation, we described a non-canonical CD95L-CD95 pathway that simultaneously drives macrophage activation, marked by high levels of IL-1β, and macrophage dysfunction, marked by the augment of CD163 in macrophages. The data showing that CD95L-CD95 signaling and IL-6 contribute to the early pulmonary inflammation point to CD95/CD95L as a therapeutic target.

RESULTS

Severe acute respiratory syndrome coronavirus 2 induces CD95/CD95L expression in airway epithelial cells

SARS-CoV-2 causes a cytopathic effect in AEC, with cytokine and chemokine secretion and caspase-8-dependent IL-1β production.[6,7] However, the mechanisms by which AEC trigger the innate response and inflammation still require a better understanding. First, we analyzed cell viability in SARS-CoV-2 (SARS2)-infected cultured Calu-3 cells, a cell line of bronchial epithelial cell, using different viral loads (MOI 0.2 and MOI 2.0). Massive cell death was detected 72 h post-infection (Figures 1A and 1B) while a significant viral load (PFU/mL) was recovered from the supernatant of infected cells at 24 and 72 h (Figure 1C). Since IL-6 is a critical mediator of immune dysregulation and severe respiratory failure,[14] we analyzed IL-6 kinetics in SARS2-infected Calu-3 cells. SARS2 at MOI 2.0 significantly induced IL-6 secretion 6 h post-infection compared to the MOI 0.2 and mock conditions. The peak of IL-6 secretion occurred 72 h post-infection (Figure 1D). Infected Calu-3 cells secreted low levels of TNF, IL-1β and IL-10 in all conditions.

Using transcriptome external databases (GSE147507),[8] we performed differential expression analysis to define differentially expressed genes (DEGs) in SARS2-infected and non-infected Calu-3 cells. The over-representation analysis (ORA) using the DEGs revealed two

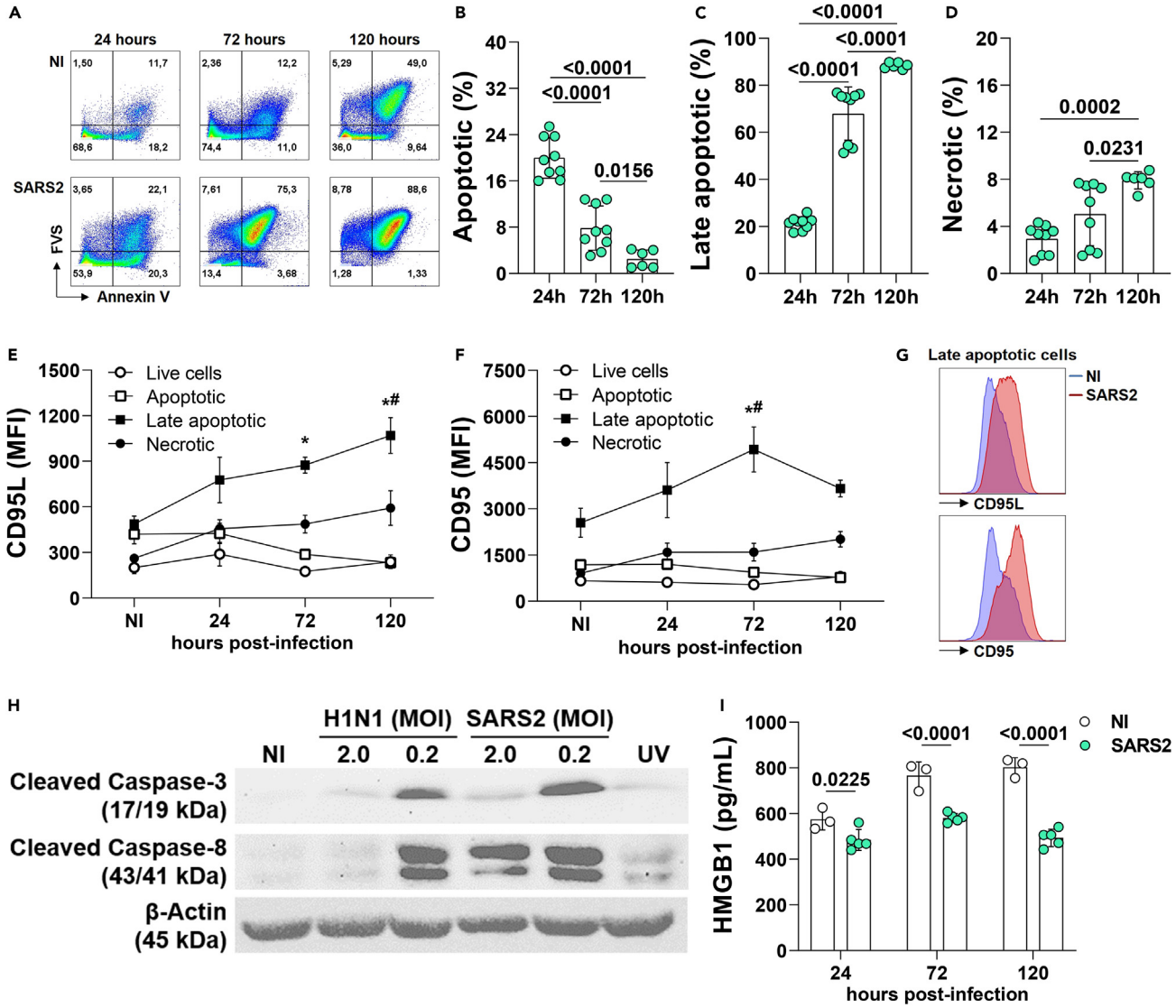

Figure 2. SARS-CoV-2 infection induces apoptosis and CD95/CD95L expression in airway epithelial cells

(A–G) Calu-3 cells were infected with SARS-CoV-2 at MOI 0.2 and evaluated by (A) flow cytometry to assess the percentage of (B) apoptotic (annexin V^+FVS^-), (C) late apoptotic (annexin V^+FVS^+) and (D) necrotic (annexin V^-FVS^+) cells after 24, 72 and 120 h p.i. The median fluorescence intensity (MFI) of (E) CD95L and (F) CD95 was determined in infected and non-infected (NI) cells and (G) represented in the histogram.

(H) Representative immunoblot image of cleaved capase-3, cleaved caspase-8 and β-actin proteins in NI cells and Calu-3 cells infected with SARS-CoV-2 and H1N1 at MOI 0.2 and 2.0 for 72 h (SARS2) or Calu-3 apoptotic cells induced by UV radiation (UV-AC, 50 mJ).

(I) HMGB1 concentration determined in the supernatants derived from NI and infected cells (SARS2) at 24, 72 and 120 h p.i. Data represent the mean ± SD of at least two independent experiments performed in triplicate. (E,F) *p < 0.05, infected vs. NI; #p < 0.05, infected vs. 24 h p.i. Bars depict the exact p values.

significantly enriched apoptotic-related pathways (Apoptotic cleavage of cellular proteins and Apoptosis) in Calu-3 cells infected with SARS2 (Figure S1). Compared to Mock, SARS2-infected Calu-3 cells showed increased expression of pro-apoptotic genes (*CASP7*, *CASP8*, *BCL2L11*, and *CD95* – Fas receptor) and decreased expression of anti-apoptotic genes (*BIRC2*), and genes related to the proteasome complex (PSM family) or to tissue damage (*HMGB1*) (Figure 1E).

Most of Calu-3 cells infected with SARS2 were in late apoptotic stage (annexin V^+FVS^+), as confirmed by flow cytometry analysis (Figures 2A–2D). A low frequency of non-infected cells was also in late apoptotic stage, as those are cultured in a medium with low fetal bovine serum (Figure 2A). At the late infection (120 h), Calu-3 cells infected with SARS2 were in necrosis compared to 24 and 72 h of infection (Figure 2D). In addition, the expression of CD95L (Fas-ligand) and CD95, determined by CD95L or CD95 median fluorescence intensity (MFI), was significantly higher only on late apoptotic cells (Figures 2E–2G). Increased expression of cleaved caspase-3 and cleaved caspase-8 were also

Table 1. Characteristics of patients with COVID-19 from whose AEC isolated from fresh tracheal aspirate were used in the analysis of CD95L expression

Demographics	All patients
Number	11
Age (yr)	58.91
Female, n (%)	6 (54.55)
Body mass index	31.33
Hospital day	30.64
Intensive care unit day	18.82
Comorbidities	
Hypertension, n (%)	9 (81.82)
Diabetes, n (%)	7 (63.64)
Obesity, n (%)	6 (54.55)
Lung disease, n (%)	0 (0.00)
History of smoking, n (%)	0 (0.00)
Laboratorial findings	
Glycemia (mg/dL)	232.00
C-reactive protein (mg/dL)	4.00
D-Dimers (μg/mL)	4.51
Ferritin (ng/mL)	2,644.80
Creatinine (mg/dL)	1.97
Urea (mg/dL)	110.14
Hemoglobin (g/dL)	11.19
Neutrophils (cell/mm^3)	15.68
Lymphocytes (cell/mm^3)	1.16
Neutrophil:Lymphocyte Ratio	23.16
Platelets (count/mm^3)	303,909
Medications	
Corticosteroid	10 (90.91)
Antibiotics	7 (63.64)
Heparin	11 (100.00)
Outcome	
PaO_2/FiO_2 Ratio	172.09
Simplified Acute Physiology Score III	58.55
Deaths	4 (36.36)

All patients had mechanical ventilation.

found in SARS2-infected Calu-3 cells (Figure 2H). The lower levels of HMGB1 in the supernatant of infected cells (Figure 2I) further support predominant cell death by apoptosis in AEC infected with SARS2.

Similar results were observed in Calu-3 cells infected with influenza A (H1N1) virus (Figure S2). H1N1 infection increased the cellular expression of cleaved caspase-3 and cleaved caspase-8, and increased IL-6 levels in the culture supernatants. In addition, most of Calu-3 cells infected with H1N1 were in late apoptotic stage (annexin V^+FVS^+) and expressed CD95L and CD95.

Apoptotic severe acute respiratory syndrome coronavirus 2-infected airway epithelial cells induces CD95 on macrophages

To investigate if AEC from patients with COVID-19 exhibit a phenotype similar to observed in Calu-3 cells, cell viability in 11 fresh tracheal aspirate samples collected from intubated patients with COVID-19 was analyzed. Clinical and laboratory characteristics of these patients are shown in Table 1. The patients, mean age was 58.9 years and 81.2% had hypertension, spent an average of 18 days in the intensive care unit (ICU), confirming severe COVID-19. Similar to observations in Calu-3 cells, most AEC from patients with COVID-19 (gated as $CD45^-EpCam^+$ cells) (Figure S3A) were dying cells (Figure 3A), exhibiting significant expression of CD95L (MFI), but not CD95, compared to live epithelial cells from the same sample (Figures 3B and 3C).

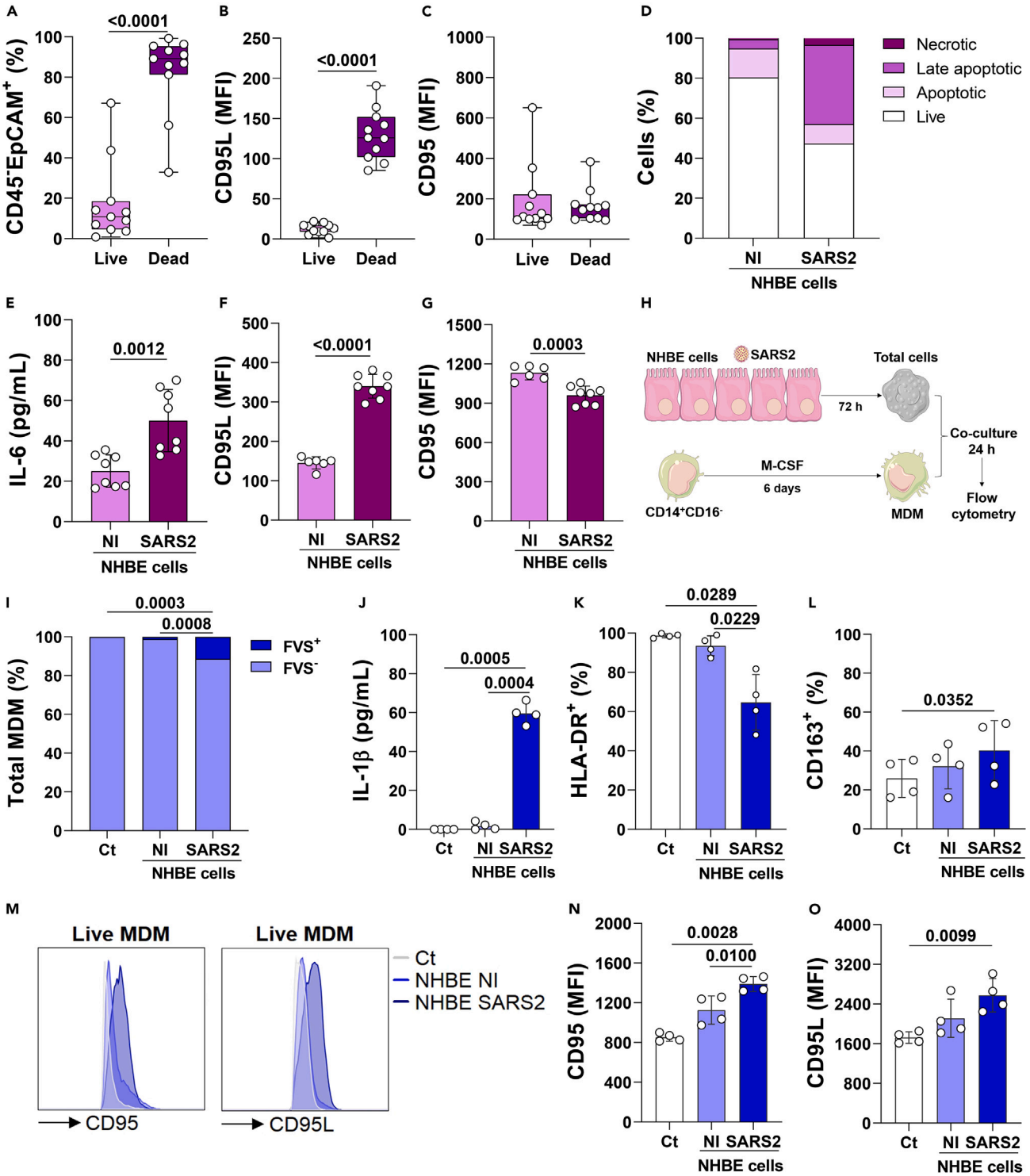

Figure 3. SARS-CoV-2-infected bronchial epithelial cells induces aberrant activation in macrophages

(A–D) Epithelial cells (CD45⁻EpCAM⁺) from tracheal aspirate of intubated patients with COVID-19 were evaluated for total (A) live or dying cells, and the median fluorescence intensity (MFI) of (B) CD95L and (C) CD95. Normal human bronchial epithelial (NHBE) cells were infected with SARS-CoV-2 at MOI 2.0 and evaluated by (D) flow cytometry to assess the percentage of live (annexin V⁻FVS⁻), apoptotic (annexin V⁺FVS⁻), late apoptotic (annexin V⁺FVS⁺) and necrotic (annexin V⁻FVS⁺) cells after 72 h p.i.

(E) IL-6 concentration was measured in the supernatants derived from non-infected (NI) and SARS2-infected NHBE cells cultures.

(F and G) The median fluorescence intensity (MFI) of (F) CD95L and (G) CD95 was determined in total cell population.

Figure 3. *Continued*

(H) Monocyte-derived macrophages (MDM, $5x10^5$/mL) were co-cultured for 24 h with total NHBE cells non-infected (NI) or infected with SARS-CoV-2 (MOI 2.0, 72 h) and compared to MDM cultured alone as control (Ct).

(I) The percentage of dying cells (FVS^+).

(J) IL-1β concentration was measured in the supernatants of co-culture.

(K and L) The percentage of (K) $HLA\text{-}DR^+$ and (L) $CD163^+$ in live MDM (FVS^-).

(M–O) (M) MFI of (N) CD95 and (O) CD95L was determined in live MDM (FVS^-).

Data represent the mean ± SD of two independent experiments. Bars depict the exact p values.

In addition to the findings in Calu-3 cells and AEC from patients with COVID-19, normal human bronchial epithelial (NHBE) cells were also dying cells (Figure 3D) and produced IL-6 in response to SARS2 infection (Figure 3E). Infected cells exhibited significant expression of CD95L (MFI), but not CD95, compared to non-infected cells (Figures 3F and 3G).

To gain insight on how dying epithelial cells directly activate macrophages during the acute phase of COVID-19, NHBE cells were infected with SARS2 (MOI 0.2 for 72 h) and co-cultured with monocyte-derived macrophages (MDM) (Figure 3H). The direct contact of MDM with SARS2-infected NHBE cells, but not with non-infected NHBE cells, significantly induced macrophage death (Figure 3I) and increased the production of IL-1β (Figure 3J). Macrophages co-cultured with SARS2-infected NHBE cells that remained alive showed reduced HLA-DR expression (Figure 3K) and increased CD163 expression (Figure 3L) compared to control macrophage cultures. Increased expression of CD95 and CD95L was observed in live macrophages (Figures 3M–3O).

These results were confirmed using sorted apoptotic Calu-3 cells 72 h post-SARS2 infection co-cultured with THP-1-derived macrophages (TDM) (Figure S4). The direct contact of macrophages with SARS2-infected apoptotic Calu-3 cells, but not with non-infected apoptotic Calu-3 cells, significantly induced macrophage death (Figures S4B and S4C). Macrophages co-cultured with apoptotic Calu-3, SARS2-infected or non-infected, that remained alive showed no alterations in HLA-DR expression compared to control macrophage culture (Figure S4D). Contact with both apoptotic cells increased CD163 expression on macrophages that remained alive (Figure S4E). Increased expression of CD95 was observed in live and dying macrophages (Figures S4F and S4G), and increased expression of CD95L was observed only in dying cells (Figures S4H and S4I).

Therefore, the direct interaction of SARS2-infected AEC with macrophages resulted in death of these innate leukocytes and positive regulation of CD95 and CD95L, mainly in dying macrophages.

IL-6 induces macrophage activation and dysfunction

Considering that SARS2-infected Calu-3 cells secrete IL-6 (Figure 1D), and IL-6 is associated with progression, severity and mortality in COVID-19,[24–26] the indirect (IL-6-mediated) effect of epithelial cells on macrophages was also investigated. The secretion of chemokines and cytokines was first determined in 28 samples of frozen tracheal aspirates collected from intubated patients with COVID-19. Clinical and laboratory characteristics of patients are shown in Table 2. The mean age was 65.29 years and 81.8% of those patients had hypertension, spent an average of 21.6 days in the ICU. IL-1β, IL-6 and TNF were the cytokines with the highest concentrations in the tracheal aspirate from these patients with COVID-19. Among those, IL-6 was detected in higher concentrations. Samples from the 28 intubated patients were divided in low (17 patients) and high (11 patients) IL-6-producers (Figure 4A). High producers showed increased levels of HMGB1 and ATP in tracheal aspirate samples compared with the low IL-6-producers (Figures 4B and 4C). Despite the increased levels of some mediators, no differences were observed in the outcome of the disease (Table 2) between low and high IL-6-producers. However, CD95L was associated with a higher incidence of death, and high IL-6-producers exhibited a significant correlation with TNF and HMGB1 (Figure 4D).

Pools of cell-free supernatants of frozen tracheal aspirate derived from low and high IL-6-producers were sorted to evaluate the effect of the inflammatory milieu on steady-state macrophages. TDM were cultured with supernatants of low or high producers of IL-6 for 24 h (Figure 4E). TDM cultured with supernatants of high IL-6-producers showed higher expression of CD95 (Figures 4F and 4G). As the median values from lower and higher IL-6-producers were 225.06 and 1,605.30 pg/mL, respectively, cultures of TDM were stimulated with recombinant human IL-6 (rIL-6) at 200 and 2,000 pg/mL to mimic low and high concentrations of IL-6. CD95 expression was greater in macrophages exposed to the higher rIL-6 concentrations (Figures 4H and 4I), similar to the observations with supernatants derived from tracheal aspirate samples.

Both supernatants, high and low IL-6-producers induced IL-1β by macrophages. High IL-6-producers induced a significant augmentation in the concentrations of IL-1β compared to stimulation in the presence of low IL-6-producers (Figure 4J). Of note, the concentrations of IL-1β in the supernatants of TDM cultures were determined subtracting the concentrations previously detected in supernatants of the tracheal aspirate. Both supernatants (high and low producers) induced decreased percentage of $HLA\text{-}DR^+$ (Figures 4K and 4M) and increased percentage of $CD163^+$ TDM (Figures 4L and 4M).

Blockade of the IL-6-CD95/CD95L axis augments HLA-DR and reduces CD163 on macrophages

To confirm that the IL-6-CD95/CD95L axis leads to the death of AEC and to both macrophage activation and dysfunction, the effects of Kp7-6 (CD95/CD95L antagonist) and tocilizumab (IL-6 receptor antagonist) were determined. Calu-3 cells treated with Kp7-6 for 2 h and then infected with SARS2 (MOI 0.2) for 24 h showed significant death reduction compared with vehicle-treated infected cells (Figure 5A).

TDM were also treated with tocilizumab 1 h before rIL-6 stimulation (Figure 5B). Considering that the severity of COVID-19 is directly correlated with high levels of IL-6[27,28] and that two patients in our cohort exhibited 3,989.82 and 3,458.98 pg/mL of IL-6 in the tracheal aspirate samples, we also tested the direct effects of rIL-6 (4,000 pg/mL) on isolated macrophages. rIL-6 increased CD95 and CD95L expression

Table 2. Characteristics of patients with COVID-19 whose tracheal aspirate supernatants were used in cultured macrophages assays

Demographics	All patients	Low IL-6	High IL-6
Number	28	17	11
Age (yr)	65.29	65.35	65.18
Female, n (%)	12 (42.85)	9 (52.94)	3 (27.27)
Body mass index	30.87	30.85	30.90
Hospital day	30.29	25.82	37.18
Intensive care unit day	21.61	19.35	25.09
Comorbidities			
Hypertension, n (%)	20 (71.43)	11 (64.71)	9 (81.82)
Diabetes, n (%)	13 (46.43)	7 (41.18)	6 (54.55)
Obesity, n (%)	15 (53.57)	9 (52.94)	6 (54.55)
Lung disease, n (%)	3 (10.71)	1 (5.88)	2 (18.18)
History of smoking, n (%)	5 (17.86)	3 (17.65)	2 (18.18)
Laboratorial findings			
Glycemia (mg/dL)	193.48	202.81	179,91
C-reactive protein (mg/dL)	11.23	7.66	16.75[a]
D-Dimers (μg/mL)	3.54	3.61	3.43
Ferritin (ng/mL)	980.67	1,096.33	826.47
Creatinine (mg/dL)	2.27	2.12	2.49
Urea (mg/dL)	122.38	133.42	105.31
Hemoglobin (g/dL)	10.79	10.92	10.58
Neutrophils (cell/mm^3)	12.09	12.86	10.88
Lymphocytes (cell/mm^3)	0.90	0.95	0.83
Neutrophil:Lymphocyte Ratio	19.85	20.83	18.33
Platelets (count/mm^3)	270,392	238,000	320,454
Medications			
Corticosteroid	19 (67.86)	12 (70.59)	7 (63.64)
Antibiotics	22 (78.57)	13 (76.47)	9 (81.82)
Heparin	27 (96.46)	16 (94.12)	11 (100.00)
Outcome			
PaO_2/FiO_2 Ratio	222.31	214.0	236.9
Simplified Acute Physiology Score III	67.41	70.82	63.55
Deaths	16 (57.15)	9 (52.94)	7 (63.64)

All patients had mechanical ventilation.
[a]$p < 0.05$ Low IL-6 vs. High IL-6, *t* test.

(Figures 5C–5E), induced the production of IL-1β (Figure 5F), decreased the expression of HLA-DR (Figure 5G) and increased the expression of CD163 on macrophages (Figure 5H). The pre-treatment with tocilizumab inhibited rIL-6 effects on TDM (Figures 5C–5H).

Next, monocyte derived macrophages (MDM) were pre-treated with tocilizumab or Kp7-6 and stimulated with rIL-6 (Figure 5I). No changes were found in CD95 expression and IL-1β was not detected in the supernatants of MDM cultures. However, MDM stimulated with rIL-6 exhibited results similar to those described for TDM: low HLA-DR expression (Figure 5J) and high CD163 expression (Figure 5K). Tocilizumab alone partially reverted the effect of rIL-6 and reduced CD163 expression, while Kp7-6 showed a more pronounced effect, with increased HLA-DR expression and decreased CD163 expression. The combined treatment, tocilizumab plus Kp7-6, produced an additional effect on the increased expression of HLA-DR and on the decreased expression of CD163 (Figures 5J and 5K).

Up regulation of MHCII on alveolar macrophages in infected CD95 deficient mice

To investigate the role of IL-6-CD95/CD95L axis *in vivo*, we used a mouse model to evaluate acute pulmonary inflammation. Although the SARS-CoV-2 infection of C57BL/6 Wild Type (WT) mice is not progressive compared to humanized ACE2 mouse, WT mouse infected with

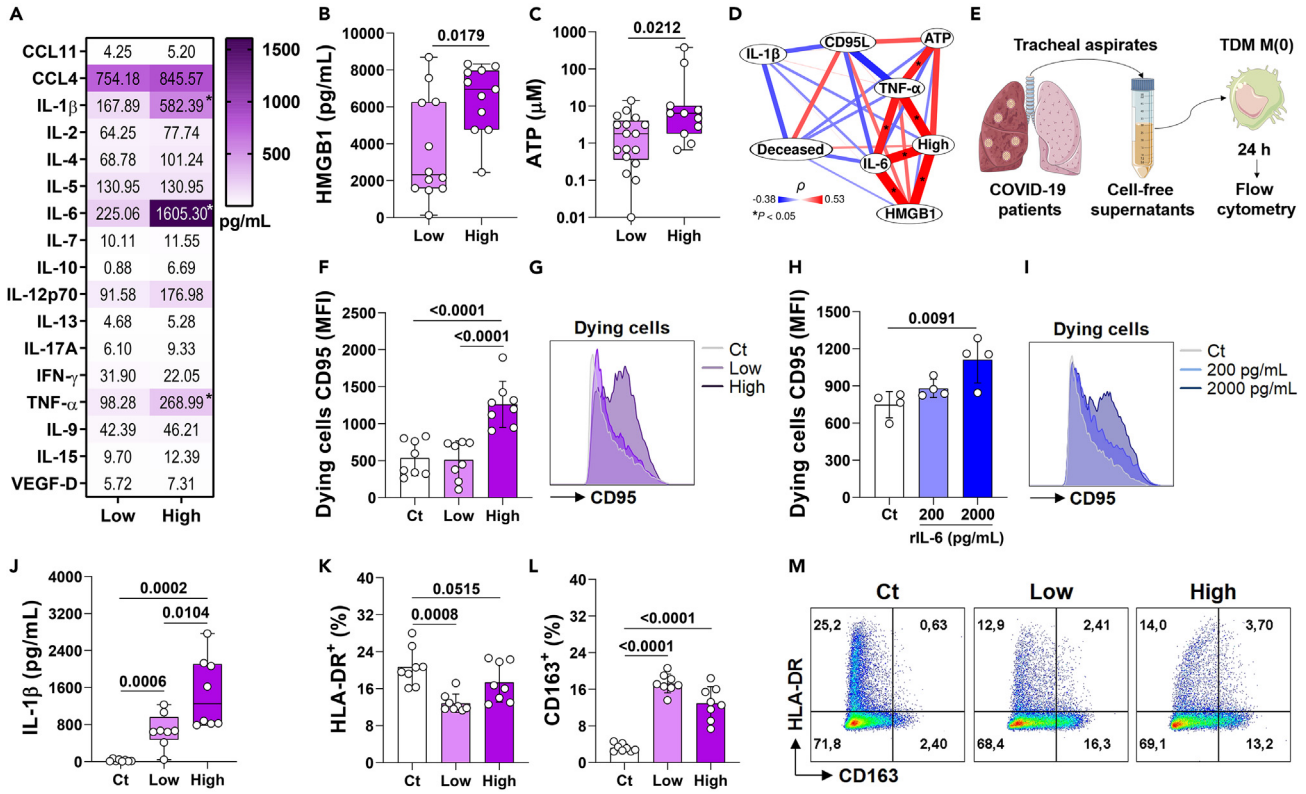

Figure 4. High IL-6 levels induce CD95 expression and IL-1β production in macrophages

(A) Inflammatory mediators were determined in tracheal aspirate samples obtained from intubated patients with COVID-19, who were sorted in pools of low and high IL-6-producers.

(B and C) Concentration of (B) HMGB1 and (C) ATP were measured in the cell-free supernatants derived from tracheal aspirate samples.

(D) Correlogram of inflammatory mediators and clinical outcomes in high IL-6-producers.

(E) THP-1-derived macrophages (TDM, 5 × 10^5/mL) were cultured for 24 h with low and high IL-6 cell-free supernatants.

(F–I) The median fluorescence intensity (MFI) of CD95 was assessed in (F and G) dying TDM (FVS^+) cultured with tracheal aspirate supernatants and in (H and I) total TDM cultured with low (200 pg/mL) and high (2000 pg/mL) concentrations of recombinant human IL-6.

(J) IL-1β detection in the supernatants and (K and M) percentage of HLA-DR and (L and M) CD163 evaluated in total live TDM (FVS^-) cultured with tracheal aspirate supernatants.

Data represent the mean ± SD of two independent experiments performed in quadruplicate for tracheal aspirate cultures and one experiment for recombinant human IL-6 cultures. (A) *p < 0.05, low vs. high; (D) *p < 0.05, Spearman's correlation. Bars depict the exact p values.

SARS-CoV-2 exhibited mild congestion and a moderate mixed inflammatory infiltrate (mononuclear cells and scarce neutrophils) associated to increased IL-6 levels in the lungs.[29] In a similar way, we observed an intense inflammatory infiltration 3 days post-infection (Figures 6A–6C) in the lungs of WT mice infected with SARS-CoV-2. CD95 (lpr) and il-6 ($il\text{-}6^{-/-}$) deficient mice showed moderate pulmonary inflammation in the lungs compared to infected WT mice (Figures 6A–6C).

SARS2 infection increased the percentage of epithelial cells (AEC - $CD45^-CD31^-EpCAM^+$) (Figure S3B) in the lungs of WT and $il\text{-}6^{-/-}$ mice compared to non-infected mice (Ct group), while infected lpr group showed no difference compared to Ct group (Figure 6D). Lpr infected mice showed a significant lower percentage of lung dying AEC, which was significantly higher in the infected WT group (Figures 6E and 6F). SARS2 infection decreased the percentage of alveolar macrophages ($CD11b^-CD11c^+SiglecF^+$ cells) that expressed MHCII in the lungs of WT mice, while an increase of both percentage and expression of MHCII (MFI) was observed in the lungs of $lpr^{-/-}$ mice (Figures 6G–6I). These findings show that CD95/CD95L signaling induces AEC death and decreases MHCII expression in alveolar macrophages.

DISCUSSION

The initial steps that orchestrate the activation of macrophages, the most abundant leukocyte in the lungs of deceased patients with COVID-19,[13] are still unknown. Using various experimental approaches, we tested the hypothesis that the death of epithelial cells triggers the inflammatory response of macrophages and generates immunopathology. In the present study we showed that the apoptosis of AEC mediated by CD95/CD95L signaling after SARS-CoV-2 infection induces both macrophage activation (production of IL-1β and expression of CD95) and macrophage dysfunction (reduction of HLA-DR and increase of CD163). In addition, macrophage dysfunction is more dependent on

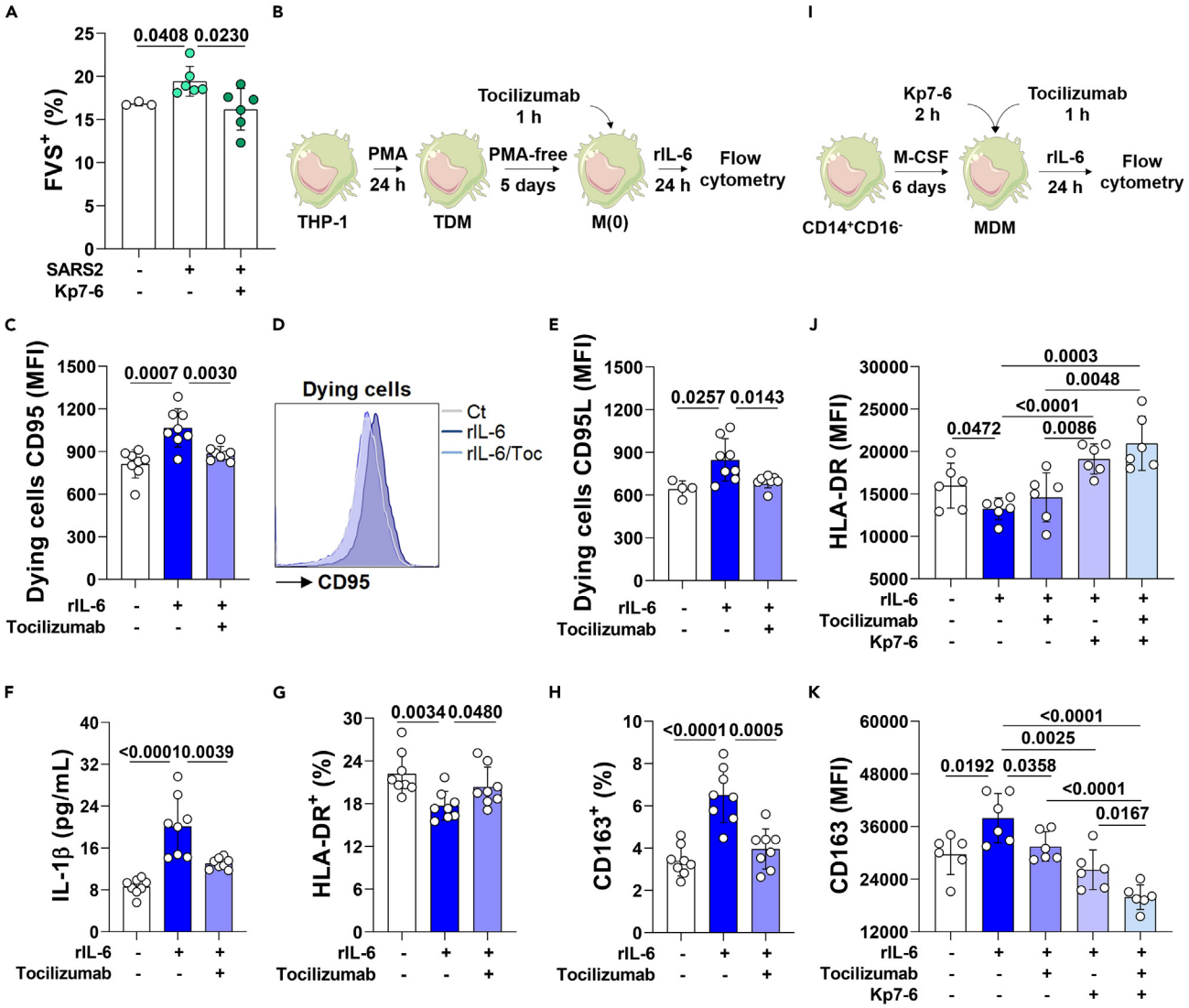

Figure 5. Blockade of IL-6 and CD95 prevents macrophage dysfunction induced by IL-6

Calu-3 cells were infected with SARS-CoV-2 at MOI 0.2 and evaluated by flow cytometry.

(A) Percentage of total dying cells (FVS^+) 24 h p.i.

(B) THP-1-derived macrophages (TDM, 5 × 10^5/mL) were cultured for 24 h with recombinant human IL-6 (4000 pg/mL) after pre-treatment with tocilizumab (100 μg/mL) for 1 h and evaluated by flow cytometry.

(C–E) The median fluorescence intensity (MFI) of (C and D) CD95 and (E) CD95L in total dying TDM (FVS^+).

(F–H) (F) IL-1β detection in the supernatants and percentage of (G) HLA-DR^+ and (H) $CD163^+$ cells evaluated in total live TDM (FVS^-).

(I) Monocyte derived macrophages (MDM, $CD14^+CD16^-$, 5 × 10^5/mL) were cultured for 24 h with recombinant human IL-6 (4000 pg/mL) after pre-treatment with Kp7-6 (100 μg/mL) for 2 h and/or with tocilizumab (100 μg/mL) for 1 h.

(J and K) Expression of HLA-DR (J) and CD163 (K) were evaluated by flow cytometry in total live human macrophages (FVS^-).

Data represent the mean ± SD of two independent experiments performed in quadruplicate (TDM) or triplicate (MDM). Bars depict the exact p values.

CD95/CD95L axis than dependent on IL-6. CD95 signaling increases the production of IL-1β, up regulates the expression of CD163 and down regulates HLA-DR (MHCII) on macrophages. Our study shows a $CD95^-$CD95L non-canonical pathway that induces activation, dysfunction and death of macrophages that trigger acute inflammation in COVID-19.

RNA viruses, such as influenza A and respiratory syncytial virus (RSV), activate CD95 (Fas) gene expression and induce apoptosis of infected cells, which favors/guarantee efficient viral egress.[30,31] Influenza virus also induces co-expression of Fas and FasL on infected cells, triggering apoptosis when the infected cells come into contact with each other.[32] These studies show that CD95/CD95L pathway might be a viral egress pathway. Our results show a similar effect of SARS-CoV-2 on Calu-3 cells and in AEC obtained from tracheal aspirates of severe patients with

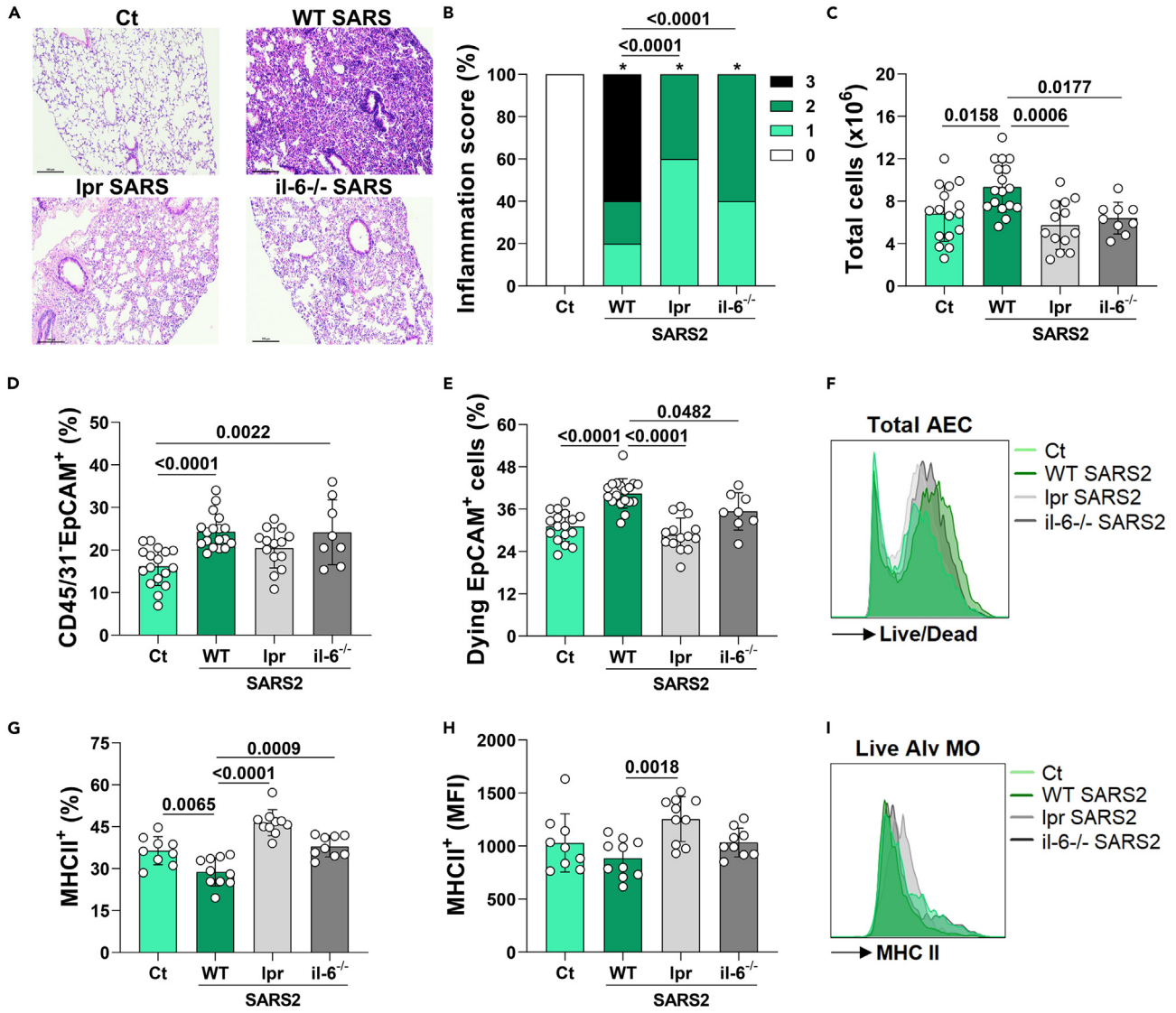

Figure 6. Lack of CD95 and IL-6 signaling reduces SARS-CoV-2-induced lung inflammation in mice

(A–C) C57BL/6 wild type (WT) and CD95 (lpr) and IL-6 (il-6$^{-/-}$) deficient mice were intranasally infected with SARS-CoV-2 (SARS2, 5 × 10^5 PFU) and evaluated 3 days post-infection. (A) Representative histopathological analysis, (B) score of inflammatory infiltration and (C) total cells count in the lungs.

(D–F) The percentage of (D) total AEC cells (CD45/31$^-$EpCAM$^+$) and (E and F) dying AEC cells (CD45/31$^-$EpCAM$^+$Live/Dead$^+$) were determined by flow cytometry.

(G–I) Live alveolar macrophages (Alv MO - L/D$^-$CD11b$^-$CD11c$^+$ SiglecF$^+$) were evaluated to assess (G) the percentage of MHCII$^+$ and (H and I) the median fluorescence intensity (MFI) of MHCII by flow cytometry.

Data represent the mean ± SD of two - four independent experiments (n = 8–16/group). Bars depict the exact p values.

COVID-19. Treatment of Calu-3 cells with CD95/CD95L antagonist decreased the number of dead cells to levels seen in untreated, non-infected cells, reinforcing that CD95/CD95L on epithelial cells is key for the process. This is an important finding considering that critical patients with COVID-19 with higher viral load remained in the ICU for shorter periods and died before critical patients in the ICU with lower viral load.[11]

However, the pro-inflammatory role of CD95/CD95L (Fas/FasL) pathway (non-canonical pathway) was described in bronchiolar epithelial cells and resulted in CXCL8 release, lung injury and pulmonary fibrosis.[33] The cytokines and chemokines released by apoptotic cells, including IL-6, CXCL8, CXCL1, CCL2, and GM-CSF, act as a "find me" signal for apoptotic cells[34] and IL-6 induction upon CD95 ligation has been described in a dose- and time-dependent manner.[35]

Here we show that CD95/CD95L pathway contributes for IL-1β released by apoptotic cells, augment of CD163 and decrease of HLA-DR on macrophages. Indeed, when we infected lpr (CD95) knockout mice, we observed reduced death of AEC and increase of MHCII on alveolar macrophages, confirming our hypothesis and reinforcing a role for the CD95/CD95L pathway on acute inflammation and macrophage dysfunction.

Our results show that the peak production of IL-6 coincided with the peak of CD95 expression in macrophages. In addition to the frequency of dying AEC, we also found increased levels of IL-6 and IL-1β in tracheal aspirates of critical patients with COVID-19.

IL-6 positively regulates the expression of CD95 on macrophages, being the expression of CD95 higher on macrophages stimulated with supernatants from high IL-6 responders. IL-6 is associated with progression, severe forms, and high mortality of disease.[36] In addition, the apoptosis of SARS-CoV-2-infected AEC, but not apoptosis of non-infected AEC, induced CD95 expression on live macrophages. These results indicate that the activation of macrophages by AEC depends on CD95 and occurs directly and indirectly: through the contact between AEC and macrophages via CD95L and CD95, respectively; and by IL-6, secreted by epithelial cells that up regulates CD95 on macrophages. As mentioned previously, CD95 may mediate non-apoptotic activities that involve cell proliferation, activation and cytokine secretion.[37,38] Cytokine secretion in MDM and in a macrophage cell lineage (RAW264.7) is independent of caspase, but relies on MyD88 and NF-κB signaling, suggesting that CD95-activated macrophages initiate and perpetuate acute inflammation and tissue injury.[39,40]

Our findings show that recombinant human IL-6 (or high levels of IL-6 from tracheal aspirates) positively regulates CD95 and CD163 expression, and reduces the expression of HLA-DR (MHCII) on macrophages. Aberrant macrophage activation described in the lungs of deceased patients with COVID-19 suggests that myeloid cells are a major source of dysregulated inflammation in COVID-19.[14,19] IL-6 is an important cytokine involved in the immunopathogenesis of COVID-19 and blockade of IL-6 signaling is considered an emerging approach.[41,42] Tocilizumab has been evaluated in at least 27 current clinical trials in COVID-19,[42] and is linked to improved clinical signs, reduced time and need for ventilation and, decreased mortality.[43–45] Here we show that CD95/CD95L antagonist played an additional effect on tocilizumab action preventing IL-6/IL6R signaling. Furthermore, using a mouse model of immunopathology, we show that CD95 exhibited a more evident role in SARS-CoV-2-induced acute lung inflammation compared to IL-6. In this way, a recent phase III trial (NCT05639192) was conducted to evaluate the efficacy of asunercept, a soluble CD95-Fc fusion protein that blocks the CD95L-CD95 interaction, for the treatment of hospitalized patients with moderate to severe COVID-19. Our findings show how CD95/CD96L contribute for macrophage dysfunction and suggest that the combined treatment of tocilizumab with asunercept may be an option for those patients who do not respond to tocilizumab alone.

Finally, our results with focus on epithelial cell and its interface with macrophage add pieces to the complex scene of COVID-19 disease, especially in the initial steps that trigger the acute inflammation that progresses to immunopathology. Our results bring a non-canonical role of CD95/CD95L signaling with the participation of IL-6, revealing CD95/CD95L as a target to be discussed as immunotherapy for the early time of severe/critical COVID-19.

Limitations of the study

Here we describe the limitations of our study. First, the clinical presentation of COVID-19 changed significantly as consequence of identified variants; here we did not focus on SARS-CoV-2 variants. Second, one of those several approaches used to validate our hypothesis was an *in vivo* model with C57BL/6 mice,[29] different from hACE2 transgenic mouse model commonly used. Because our aim was to measure the hallmarks of initial inflammation, AEC death and macrophage dysfunction, but not viral progression, this mouse model was suitable for our purpose. Third, although our results are robust, we were not able to confirm those results in lung biopsies.

STAR★METHODS

Detailed methods are provided in the online version of this paper and include the following:

- Transcriptome analysis
- Statistical analysis and figures

SUPPLEMENTAL INFORMATION

Supplemental information can be found online at https://doi.org/10.1016/j.isci.2023.108366.

ACKNOWLEDGMENTS

The authors are thankful to Ana Flavia Gembre, Denise Brufato Ferraz and Denise Ferro for excellent technical support and to Iris Castro for help with flow cytometry. This study was supported by the São Paulo Research Foundation (FAPESP), grants 2020/05270-0 and 2019/11213-1 to VLDB and grant 2019/09881-6 to TFCF-S, and to the Brazilian National Council for Scientific and Technological Development (CNPq), grants 312606/2019-2 and 402367/2022-7 to MDB.

AUTHOR CONTRIBUTIONS

Conceptualization, T.F.C.F.-S. and V.L.D.B.; methodology, T.F.C.F.-S. and V.L.D.B. Formal analysis, T.F.C.F.-S. and C.A.F.; investigation, T.F.C.F.-S., U.G.C., M.J.F., G.F.C., D.d-S., and F.L.A.C.M.; resources, C.B., A.T.-C., J.C.-R., M.G.M., L.T.M.F., L.D.C., O.A.M.-F., M.D.-B., M.A.-M., R.T., and V.L.D.B.; writing – original draft, T.F.C.F.-S. and V.L.D.B.; writing – review & editing, T.F.C.F.-S., L.D.C., M.D.-B., R.T., and V.L.D.B.; supervision, V.L.D.B.; project administration, T.F.C.F.-S. and V.L.D.B.; funding acquisition, V.L.D.B.

DECLARATION OF INTERESTS

The authors declare no competing interests.

INCLUSION AND DIVERSITY

We support inclusive, diverse, and equitable conduct of research.

Received: October 7, 2022
Revised: September 9, 2023
Accepted: October 26, 2023
Published: October 31, 2023

REFERENCES

1. Sungnak, W., Huang, N., Bécavin, C., Berg, M., Queen, R., Litvinukova, M., Talavera-López, C., Maatz, H., Reichart, D., Sampaziotis, F., et al. (2020). SARS-CoV-2 entry factors are highly expressed in nasal epithelial cells together with innate immune genes. Nat. Med. *26*, 681–687.
2. Hou, Y.J., Okuda, K., Edwards, C.E., Martinez, D.R., Asakura, T., Dinnon, K.H., Kato, T., Lee, R.E., Yount, B.L., Mascenik, T.M., et al. (2020). SARS-CoV-2 Reverse Genetics Reveals a Variable Infection Gradient in the Respiratory Tract. Cell *182*, 429–446.e14.
3. Grant, R.A., Morales-Nebreda, L., Markov, N.S., Swaminathan, S., Querrey, M., Guzman, E.R., Abbott, D.A., Donnelly, H.K., Donayre, A., Goldberg, I.A., et al. (2021). Circuits between infected macrophages and T cells in SARS-CoV-2 pneumonia. Nature *590*, 635–641.
4. Ziegler, C.G.K., Allon, S.J., Nyquist, S.K., Mbano, I.M., Miao, V.N., Tzouanas, C.N., Cao, Y., Yousif, A.S., Bals, J., Hauser, B.M., et al. (2020). SARS-CoV-2 Receptor ACE2 Is an Interferon-Stimulated Gene in Human Airway Epithelial Cells and Is Detected in Specific Cell Subsets across Tissues. Cell *181*, 1016–1035.e19.
5. Varga, Z., Flammer, A.J., Steiger, P., Haberecker, M., Andermatt, R., Zinkernagel, A.S., Mehra, M.R., Schuepbach, R.A., Ruschitzka, F., and Moch, H. (2020). Endothelial cell infection and endotheliitis in COVID-19. Lancet *395*, 1417–1418.
6. Zhu, N., Zhang, D., Wang, W., Li, X., Yang, B., Song, J., Zhao, X., Huang, B., Shi, W., Lu, R., et al. (2020). A novel coronavirus from patients with pneumonia in China, 2019. N. Engl. J. Med. *382*, 727–733.
7. Li, S., Zhang, Y., Guan, Z., Li, H., Ye, M., Chen, X., Shen, J., Zhou, Y., Shi, Z.L., Zhou, P., and Peng, K. (2020). SARS-CoV-2 triggers inflammatory responses and cell death through caspase-8 activation. Signal Transduct. Target. Ther. *5*, 235. https://doi.org/10.1038/s41392-020-00334-0.
8. Blanco-Melo, D., Nilsson-Payant, B.E., Liu, W.C., Uhl, S., Hoagland, D., Møller, R., Jordan, T.X., Oishi, K., Panis, M., Sachs, D., et al. (2020). Imbalanced Host Response to SARS-CoV-2 Drives Development of COVID-19. Cell *181*, 1036–1045.e9.
9. Schulte-Schrepping, J., Reusch, N., Paclik, D., Baßler, K., Schlickeiser, S., Zhang, B., Krämer, B., Krammer, T., Brumhard, S., Bonaguro, L., et al. (2020). Severe COVID-19 Is Marked by a Dysregulated Myeloid Cell Compartment. Cell *182*, 1419–1440.e23.
10. Fraga-Silva, T.F.d.C., Maruyama, S.R., Sorgi, C.A., Russo, E.M.d.S., Fernandes, A.P.M., de Barros Cardoso, C.R., Faccioli, L.H., Dias-Baruffi, M., and Bonato, V.L.D. (2020). COVID-19: Integrating the Complexity of Systemic and Pulmonary Immunopathology to Identify Biomarkers for Different Outcomes. Front. Immunol. *11*, 599736. https://doi.org/10.3389/fimmu.2020.599736.
11. Nienhold, R., Ciani, Y., Koelzer, V.H., Tzankov, A., Haslbauer, J.D., Menter, T., Schwab, N., Henkel, M., Frank, A., Zsikla, V., et al. (2020). Two distinct immunopathological profiles in autopsy lungs of COVID-19. Nat. Commun. *11*, 5086.
12. Desai, N., Neyaz, A., Szabolcs, A., Shih, A.R., Chen, J.H., Thapar, V., Nieman, L.T., Solovyov, A., Mehta, A., Lieb, D.J., et al. (2020). Temporal and spatial heterogeneity of host response to SARS-CoV-2 pulmonary infection. Nat. Commun. *11*, 6319.
13. Dorward, D.A., Russell, C.D., Um, I.H., Elshani, M., Armstrong, S.D., Penrice-Randal, R., Millar, T., Lerpiniere, C.E.B., Tagliavini, G., Hartley, C.S., et al. (2021). Tissue-specific Immunopathology in Fatal COVID-19. Am. J. Respir. Crit. Care Med. *203*, 192–201.
14. Giamarellos-Bourboulis, E.J., Netea, M.G., Rovina, N., Akinosoglou, K., Antoniadou, A., Antonakos, N., Damoraki, G., Gkavogianni, T., Adami, M.E., Katsaounou, P., et al. (2020). Complex Immune Dysregulation in COVID-19 Patients with Severe Respiratory Failure. Cell Host Microbe *27*, 992–1000.e3.
15. Veras, F.P., Pontelli, M.C., Silva, C.M., Toller-Kawahisa, J.E., de Lima, M., Nascimento, D.C., Schneider, A.H., Caetité, D., Tavares, L.A., Paiva, I.M., et al. (2020). SARS-CoV-2–triggered neutrophil extracellular traps mediate COVID-19 pathology. J. Exp. Med. *217*, e20201129. https://doi.org/10.1084/jem.20201129.

16. Bellesi, S., Metafuni, E., Hohaus, S., Maiolo, E., Marchionni, F., D'Innocenzo, S., La Sorda, M., Ferraironi, M., Ramundo, F., Fantoni, M., et al. (2020). Increased CD95 (Fas) and PD-1 expression in peripheral blood T lymphocytes in COVID-19 patients. Br. J. Haematol. *191*, 207–211.
17. Neidleman, J., Luo, X., George, A.F., McGregor, M., Yang, J., Yun, C., Murray, V., Gill, G., Greene, W.C., Vasquez, J., et al. (2021). Distinctive features of SARS-CoV-2-specific T cells predict recovery from severe COVID-19. Cell Rep. *36*, 109414.
18. Bhattacharya, M. (2022). Insights from Transcriptomics: CD163 + Profibrotic Lung Macrophages in COVID-19. Am. J. Respir. Cell Mol. Biol. *67*, 520–527.
19. Melms, J.C., Biermann, J., Huang, H., Wang, Y., Nair, A., Tagore, S., Katsyv, I., Rendeiro, A.F., Amin, A.D., Schapiro, D., et al. (2021). A molecular single-cell lung atlas of lethal COVID-19. Nature *595*, 114–119.
20. Lian, Q., Zhang, K., Zhang, Z., Duan, F., Guo, L., Luo, W., Mok, B.W.Y., Thakur, A., Ke, X., Motallebnejad, P., et al. (2022). Differential effects of macrophage subtypes on SARS-CoV-2 infection in a human pluripotent stem cell-derived model. Nat. Commun. *13*, 2028.
21. Benlyamani, I., Venet, F., Coudereau, R., Gossez, M., and Monneret, G. (2020). Monocyte HLA-DR Measurement by Flow Cytometry in COVID -19 Patients: An Interim Review. Cytometry A. *97*, 1217–1221.
22. Lucas, C., Wong, P., Klein, J., Castro, T.B.R., Silva, J., Sundaram, M., Ellingson, M.K., Mao, T., Oh, J.E., Israelow, B., et al. (2020). Longitudinal analyses reveal immunological misfiring in severe COVID-19. Nature *584*, 463–469.
23. Salina, A.C.G., Dos-Santos, D., Rodrigues, T.S., Fortes-Rocha, M., Freitas-Filho, E.G., Alzamora-Terrel, D.L., Castro, I.M.S., Fraga da Silva, T.F.C., de Lima, M.H.F., Nascimento, D.C., et al. (2022). Efferocytosis of SARS-CoV-2-infected dying cells impairs macrophage anti-inflammatory functions and clearance of apoptotic cells. Elife *11*, e74443. https://doi.org/10.7554/eLife.74443.
24. Ulhaq, Z.S., and Soraya, G.V. (2020). Interleukin-6 as a potential biomarker of COVID-19 progression. Med. Mal. Infect. *50*, 382–383.
25. Mojtabavi, H., Saghazadeh, A., and Rezaei, N. (2020). Interleukin-6 and severe COVID-19: a systematic review and meta-analysis. Eur. Cytokine Netw. *31*, 44–49.
26. Gorham, J., Moreau, A., Corazza, F., Peluso, L., Ponthieux, F., Talamonti, M., Izzi, A., Nagant, C., Ndieugnou Djangang, N., Garufi, A., et al. (2020). Interleukine-6 in critically ill COVID-19 patients: A retrospective analysis. PLoS One *15*, e0244628.
27. Han, H., Ma, Q., Li, C., Liu, R., Zhao, L., Wang, W., Zhang, P., Liu, X., Gao, G., Liu, F., et al. (2020). Profiling serum cytokines in COVID-19 patients reveals IL-6 and IL-10 are disease severity predictors. Emerg. Microbes Infect. *9*, 1123–1130.
28. Liu, J., Li, S., Liu, J., Liang, B., Wang, X., Wang, H., Li, W., Tong, Q., Yi, J., Zhao, L., et al. (2020). Longitudinal characteristics of lymphocyte responses and cytokine profiles in the peripheral blood of SARS-CoV-2 infected patients. EBioMedicine *55*, 102763. https://doi.org/10.1016/j.ebiom.2020.102763.
29. Fumagalli, M.J., Castro-Jorge, L.A., Fraga-Silva, T.F.d.C., de Azevedo, P.O., Capato, C.F., Rattis, B.A.C., Hojo-Souza, N.S., Floriano, V.G., de Castro, J.T., Ramos, S.G., et al. (2021). Protective Immunity against Gamma and Zeta Variants after Inactivated SARS-CoV-2 Virus Immunization. Viruses *13*, 2440.
30. Ampomah, P.B., and Lim, L.H.K. (2020). Influenza A virus-induced apoptosis and virus propagation. Apoptosis *25*, 1–11.
31. O'Donnell, D.R., Milligan, L., and Stark, J.M. (1999). Induction of CD95 (Fas) and Apoptosis in Respiratory Epithelial Cell Cultures Following Respiratory Syncytial Virus Infection. Virology *257*, 198–207.
32. Fujimoto, I., Takizawa, T., Ohba, Y., and Nakanishi, Y. (1998). Co-expression of Fas and Fas-ligand on the surface of influenza virus-infected cells. Cell Death Differ. *5*, 426–431.
33. Hagimoto, N., Kuwano, K., Kawasaki, M., Yoshimi, M., Kaneko, Y., Kunitake, R., Maeyama, T., Tanaka, T., and Hara, N. (1999). Induction of Interleukin-8 Secretion and Apoptosis in Bronchiolar Epithelial Cells by Fas Ligation. Am. J. Respir. Cell Mol. Biol. *21*, 436–445.
34. Cullen, S.P., Henry, C.M., Kearney, C.J., Logue, S.E., Feoktistova, M., Tynan, G.A., Lavelle, E.C., Leverkus, M., and Martin, S.J. (2013). Fas/CD95-Induced Chemokines Can Serve as "Find-Me" Signals for Apoptotic Cells. Mol. Cell *49*, 1034–1048.
35. Choi, C., Gillespie, G.Y., Van Wagoner, N.J., and Benveniste, E.N. (2002). Fas engagement increases expression of interleukin-6 in human glioma cells. J. Neuro Oncol. *56*, 13–19.
36. Liu, X., Wang, H., Shi, S., and Xiao, J. (2022). Association between IL-6 and severe disease and mortality in COVID-19 disease: a systematic review and meta-analysis. Postgrad. Med. J. *98*, 871–879. postgradmedj-2021-139939.
37. Peter, M.E., Budd, R.C., Desbarats, J., Hedrick, S.M., Hueber, A.-O., Newell, M.K., Owen, L.B., Pope, R.M., Tschopp, J., Wajant, H., et al. (2007). The CD95 Receptor: Apoptosis Revisited. Cell *129*, 447–450.
38. Guégan, J.P., Ginestier, C., Charafe-Jauffret, E., Ducret, T., Quignard, J.-F., Vacher, P., and Legembre, P. (2020). CD95/Fas and metastatic disease: What does not kill you makes you stronger. Semin. Cancer Biol. *60*, 121–131.
39. Park, D.R., Thomsen, A.R., Frevert, C.W., Pham, U., Skerrett, S.J., Kiener, P.A., and Liles, W.C. (2003). Fas (CD95) Induces Proinflammatory Cytokine Responses by Human Monocytes and Monocyte-Derived Macrophages. J. Immunol. *170*, 6209–6216.
40. Altemeier, W.A., Zhu, X., Berrington, W.R., Harlan, J.M., and Liles, W.C. (2007). Fas (CD95) induces macrophage proinflammatory chemokine production via a MyD88-dependent, caspase-independent pathway. J. Leukoc. Biol. *82*, 721–728.
41. Jones, S.A., and Hunter, C.A. (2021). Is IL-6 a key cytokine target for therapy in COVID-19? Nat. Rev. Immunol. *21*, 337–339.
42. Elahi, R., Karami, P., Heidary, A.H., and Esmaeilzadeh, A. (2022). An updated overview of recent advances, challenges, and clinical considerations of IL-6 signaling blockade in severe coronavirus disease 2019 (COVID-19). Int. Immunopharmacol. *105*, 108536.
43. Canziani, L.M., Trovati, S., Brunetta, E., Testa, A., De Santis, M., Bombardieri, E., Guidelli, G., Albano, G., Folci, M., Squadroni, M., et al. (2020). Interleukin-6 receptor blocking with intravenous tocilizumab in COVID-19 severe acute respiratory distress syndrome: A retrospective case-control survival analysis of 128 patients. J. Autoimmun. *114*, 102511.
44. Kewan, T., Covut, F., Al–Jaghbeer, M.J., Rose, L., Gopalakrishna, K.V., and Akbik, B. (2020). Tocilizumab for treatment of patients with severe COVID–19: A retrospective cohort study. EClinicalMedicine *24*, 100418.
45. Kaye, A.G., and Siegel, R. (2020). The efficacy of IL-6 inhibitor Tocilizumab in reducing severe COVID-19 mortality: a systematic review. PeerJ *8*, e10322.
46. Araujo, D.B., Machado, R.R.G., Amgarten, D.E., Malta, F.d.M., de Araujo, G.G., Monteiro, C.O., Candido, E.D., Soares, C.P., de Menezes, F.G., Pires, A.C.C., et al. (2020). SARS-CoV-2 isolation from the first reported patients in Brazil and establishment of a coordinated task network. Mem. Inst. Oswaldo Cruz *115*, e200342. https://doi.org/10.1590/0074-02760200342.
47. Baxter, E.W., Graham, A.E., Re, N.A., Carr, I.M., Robinson, J.I., Mackie, S.L., and Morgan, A. (2020). Standardized protocols for differentiation of THP-1 cells to macrophages with distinct M(IFNγ+LPS), M(IL-4) and M(IL-10) phenotypes. J. Immunol. Methods *478*, 112721.
48. Hoepel, W., Chen, H.-J., Geyer, C.E., Allahverdiyeva, S., Manz, X.D., de Taeye, S.W., Aman, J., Mes, L., Steenhuis, M., Griffith, G.R., et al. (2021). High titers and low fucosylation of early human anti–SARS-CoV-2 IgG promote inflammation by alveolar macrophages. Sci. Transl. Med. *13*, eabf8654. https://doi.org/10.1126/scitranslmed.abf8654.
49. Hasegawa, A., Cheng, X., Kajino, K., Berezov, A., Murata, K., Nakayama, T., Yagita, H., Murali, R., and Greene, M.I. (2004). Fas-disabling small exocyclic peptide mimetics limit apoptosis by an unexpected mechanism. Proc. Natl. Acad. Sci. USA *101*, 6599–6604.
50. Edgar, R., Domrachev, M., and Lash, A.E. (2002). Gene Expression Omnibus: NCBI gene expression and hybridization array data repository. Nucleic Acids Res. *30*, 207–210.
51. Benjamini, Y., and Hochberg, Y. (1995). Controlling the False Discovery Rate: A Practical and Powerful Approach to Multiple Testing. J. R. Stat. Soc. Ser. B *57*, 289–300.

STAR★METHODS

KEY RESOURCES TABLE

REAGENT or RESOURCE	SOURCE	IDENTIFIER
Antibodies		
CD95 PerCP eFluor-710 (APO-1/Fas, DX2)	eBioscience, USA	Cat# 46-0959-42; RRID:AB_10670078
CD45 PE-Cy7 (2D1)	eBioscience, USA	Cat# 25-9459-42; RRID:AB_2573544
HLA-DR PE-Cy7 (LN3)	eBioscience, USA	Cat# 25-9956-42; RRID:AB_1582284
CD163 PE (GHI/61)	eBioscience, USA	Cat# 12-1639-42; RRID:AB_1963570
CD163 APC (GHI/61)	eBioscience, USA	Cat# 17-1639-42; RRID:AB_2573168
CD178 APC (CD95L, Fas-ligand, NOK-1)	BD Biosciences, USA	Cat# 564262; RRID:AB_2738714
EpCAM PE (EBA-1)	BD Biosciences, USA	Cat# 347198; RRID:AB_400262
HLA-DR BB700 (G46-6)	BD Biosciences, USA	Cat# 566480; RRID:AB_2744477
CD45 PE-Cy7 (30-F11)	BD Biosciences, USA	Cat# 552848; RRID:AB_394489
CD31 PE-Cy7 (390)	BD Biosciences, USA	Cat# 561410; RRID:AB_10612003
CD326 BB515 (EpCAM, G8.8)	BD Biosciences, USA	Cat# 565425; RRID:AB_2739232
CD11b BV711 (M1/70)	BD Biosciences, USA	Cat# 563168; RRID:AB_2716860
CD11c PE-Cy7 (HL3)	BD Biosciences, USA	Cat# 558079; RRID:AB_647251
SiglecF BB515 (E50-2440)	BD Biosciences, USA	Cat# 564514; RRID:AB_2738833
MHCII BB700 (IA/IE, M5/114.15.2)	BD Biosciences, USA	Cat# 746197; RRID:AB_2743544
Cleaved Caspase-3 (Asp175) (5A1E) Rabbit mAb	Cell Signaling, USA	Cat# 9664; RRID:AB_2070042
Cleaved Caspase-8 (Asp374) (18C8) Rabbit mAb	Cell Signaling, USA	Cat# 9496
β-Actin (8H10D10) Mouse mAb (HRP Conjugate)	Cell Signaling, USA	Cat# 12262; RRID:AB_2566811
Bacterial and virus strains		
Wild type SARS-CoV-2	University of Sao Paulo, SP, Brazil	GenBank access MT126808.1
Influenza A virus (H1N1)	University of Sao Paulo, SP, Brazil	Strain A/California/17/2009pdm(H1N1)
Biological samples		
Tracheal aspirates collected from intubated COVID-19 patients	University of Sao Paulo, SP, Brazil	N/A
Chemicals, peptides, and recombinant proteins		
Trypsin/EDTA	Lonza, USA	Cat# CC-5012
Phorbol 12-Myristate 13-Acetate	Sigma-Aldrich, USA	Cat# P8139
kp7-6 (CD95/CD95L antagonist)	Sigma-Aldrich, USA	Cat# 341291
Recombinant Human M-CSF	PeproTech, USA	Cat# 300–25
Recombinant Human IL-6	PeproTech, USA	Cat# 200–06
Tocilizumab	Roche, Switzerland	Actemra
Critical commercial assays		
Human IL-6 DuoSet ELISA	R&D System, USA	Cat# DY206
Human IL-1 beta/IL-1F2 DuoSet ELISA	R&D System, USA	Cat# DY201
Human TNF-alpha DuoSet ELISA	R&D System, USA	Cat# DY210
Human IL-10 DuoSet ELISA	R&D System, USA	Cat# DY217B
Bio-Plex Pro Human Cytokine 27-plex Assay	Bio-Rad, USA	Cat# M500KCAF0Y
Human HMGB1/HMG-1 ELISA Kit	NOVUS Biologicals, USA	Cat# NBP2-62766
Adenosine 5′-triphosphate (ATP) Bioluminescent Assay Kit	Sigma-Aldrich, USA	Cat# FLAA
Fixable Violet Dead Cell Stain Kit	Invitrogen, USA	Cat# L34955

(*Continued on next page*)

Continued

REAGENT or RESOURCE	SOURCE	IDENTIFIER
Annexin V Apoptosis Detection Kits	BD Biosciences, USA	Cat# 88-8103-74
Fixable Viability Stain 780	BD Biosciences, USA	Cat# 565388
Classical Monocyte Isolation kit human	Miltenyi Biotec, USA	Cat# 130-117-337
Experimental models: Cell lines		
Vero E6	American Type Culture Collection, USA	Cat# CRL-1586, RRID:CVCL_0574
NHBE	Lonza, USA	Cat# CC-2541
Calu-3	Cell Bank of Rio de Janeiro – BCRJ, Brazil	Cat# BCRJ 0264; RRID:CVCL_0609
THP-1	Cell Bank of Rio de Janeiro – BCRJ, Brazil	Cat# BCRJ 0234; RRID:CVCL_0006
Experimental models: Organisms/strains		
C57BL/6 mice	University of Sao Paulo, SP, Brazil	RRID:MGI:2159769
CD95 (lpr) deficient mice	University of Sao Paulo, SP, Brazil	N/A
IL-6 (il-6$^{-/-}$) deficient mice	University of Sao Paulo, SP, Brazil	N/A
Software and algorithms		
GraphPad Prism 8.0.2	GraphPad Prism	https://www.graphpad.com/
The R environment	The R Project for Statistical Computing	https://www.R-project.org/
Other		
Dulbecco's Modified Eagle's Medium (DMEM, 1 g/L D-glucose)	Gibco, USA	Cat# 11885–084
Dulbecco's Modified Eagle's Medium (DMEM, 4.5 g/L D-glucose)	Gibco, USA	Cat# 11965–092
Fetal Bovine Serum	Gibco, Brazil	Cat# 12657–029
Penicillin-Streptomycin (10,000 U/mL)	Gibco, USA	Cat# 15140122
Sodium Pyruvate (100 mM)	Gibco, China	Cat# 11360070
MEM Non-Essential Amino Acids Solution (100X)	Gibco, USA	Cat# 11140050
L-Glutamine (200 mM)	Gibco, Brazil	Cat# 25030081
Iscove's Modified Dulbecco's Medium (IMDM)	HyClone, USA	Cat# SH30228.01
Bronchial Epithelial Cell Basal Medium (BEBM)	Lonza, USA	Cat# CC-3171
Bronchial Epithelial Cell Growth Medium (BEGM)	Lonza, USA	Cat# CC-4175

RESOURCE AVAILABILITY

Lead contact

Further information and requests for resources and reagents should be directed to and will be fulfilled by the lead contact, Vania Bonato (vlbonato@fmrp.usp.br).

Materials availability

This study did not generate new unique reagents.

Data and code availability

Raw data generated in this study are available after registration at https://repositorio.uspdigital.usp.br/handle/item/571. The raw sequencing external datasets using in this study are available on the NCBI Gene Expression Omnibus (GEO) server under the accession number GSE147507. This paper does not report original code. Any additional information required to reanalyze the data reported in this paper is available from the lead contact upon request.

EXPERIMENTAL MODEL AND STUDY PARTICIPANT DETAILS

Study participants

The COVID-19 group included 39 Brazilians citizens, female and male, 35–87 years old (Tables 1 and 2), who were admitted to the Intensive Care Unit (ICU) of the Clinics Hospital of Ribeirao Preto of the University of Sao Paulo and need mechanical ventilation. COVID-19 infection

was confirmed by a positive RT-PCR test. This study was approved by the local Ethic Committee (CAAE: 30816620.0.0000.5440). All participants or family members have provided informed consent.

Animals

Six weeks old female C57BL/6 wild type (WT) and CD95 (lpr) and IL-6 (il-6$^{-/-}$) deficient mice were used for SARS-CoV-2 infection of the Clinics Hospital of Ribeirao Preto of the University of Sao Paulo (SP, Brazil). Animals were obtained from the breeding facility of Ribeirao Preto Medical School, University of Sao Paulo (Ribeirao Preto, SP, Brazil). All animals were maintained in sterile environmental conditions in a ventilated rack (Alesco, Monte Mor, SP, Brazil) and received sterile food and water. All experiments were performed according to the local Ethics Committee on Animal Experimentation (Protocol Number 114/2021).

METHOD DETAILS

Sample collection

Tracheal aspirate samples (2–5 mL) were collected by aspiration into sterile tracheal secretion collectors in the early morning routine visit of patients for airway cleansing and only productive secretion was used in this study. Tracheal aspirate samples were manipulated in a biosafety level 3 laboratory (Department of Biochemistry and Immunology, Ribeirao Preto Medical School, University of Sao Paulo, Ribeirao Preto, Sao Paulo, Brazil) in 2 h post collection. All sample were diluted in 1:2 in phosphate buffered saline (PBS) and filtered through cell strainers (70 μm) into polypropylene tubes to remove mucous clumps and cell aggregates. Samples were further centrifuged at 24,000 × g and filtered through 0.45 μm syringe filter to assess cell-free supernatants.

SARS-CoV-2 and H1N1

The WT SARS-CoV-2 virus (GenBank access MT126808.1) was isolated from clinical samples in Brazil.[46] Viral stocks were propagated in African green monkey kidney epithelial (Vero E6) cells cultured with Dulbecco's Modified Eagle's Medium (DMEM, Gibco) supplemented with 1% penicillin/streptomycin and 2% Fetal Bovine Serum (FBS, Gibco) and maintained at 37°C and 5% CO2 and viral titration was performed by plaque assay.[46] For viral RNA quantification, RNA was extracted with TRIzol (Thermo, USA) reagent with 20 mg of lung homogenate, according to manufacturer's recommendation and qRT-PCR was performed using TaqMan Fast Virus 1-Step Mix (Applied Biosystems, USA) according to the manufacturer's recommendations. SARS-CoV-2 primers and probe were designed to target a 100 bp region from RNA-dependent-RNA polymerase gene (RdRp) of all three SARS-CoV-2 variants (Forward: 5′ – GTGAAATGGTCATGTGTGGCGG – 3′; Reverse: 5′ – CAAA TGTTAAAAACACTATTAGCATA – 3′ and Probe: '5-FAM – CAGGTGGAACCTCATCAGGAGATGC – BHQ1-3') and the reactions were performed using a StepOnePlus Real-Time PCR system (Applied Biossystems), according.[29] Influenza A virus (H1N1), strain A/California/17/2009pdm(H1N1), was gently provided by Professor Edison Durigon (University of Sao Paulo, SP, Brazil).

Cell lines

Human adenocarcinoma lung epithelial cell line (Calu-3, BCRJ 0264) and a human leukemia monocytic cell line (THP-1, BCRJ 0234) were maintained at 37°C and 5% CO2 in DMEM (1 g/L D-glucose, GIBCO) supplemented with 20% fetal bovine serum (FBS, Gibco) and 1% penicillin/streptomycin (Gibco). Calu-3 infection with SARS-CoV-2 and H1N1 was performed at an MOI of 0.2 or 2.0 in DMEM (4.5 g/L D-glucose, GIBCO) supplemented with 2% FBS, 1% penicillin/streptomycin, 4 mM L-glutamine, 10 mM non-essential amino acids and 1 mM sodium pyruvate. THP-1 cells were differentiated into a macrophage-like phenotype (TDM, THP-1-derived macrophages) using phorbol-12-myristate-13-acetate (PMA, 5 ng/mL, Sigma) for 24 h and 5 days for rest period in PMA-free medium, as defined by Baxter et al.[47] Then, TDM was co-cultured with apoptotic Calu-3, stimulated with 50% cell-free supernatants derived from tracheal aspirate of patients or stimulated with recombinant human IL-6.

Human primary cells

Normal Human Bronchial Epithelial cells (NHBE, Lonza CC-2541) were cultured in Bronchial Epithelial Cell Growth Medium (BEGM, Lonza) and infected with SARS-CoV-2 at an MOI of 2.0 for 72 h at 37°C and 5% CO_2. Human monocytes were differentiated into a macrophage-like phenotype (MDM, monocyte-derived macrophages) using M-CSF (50 ng/mL, Peprotech) for 6 days at 37°C and 5% CO_2 in Iscove's Modified Dulbecco's Medium (IMDM, HyClone) supplemented with 5% FBS and 1% penicillin/streptomycin, adapted from.[48] Monocytes ($CD14^+CD16^-$) were sorted by columns with magnetic beads (Miltenyi Biotec, Germany) from total mononuclear cells isolated by Ficoll gradient from the peripheral blood of healthy volunteers. Total SARS-CoV-2-infected NHBE cells were then co-cultured with MDM for 24 h in an equal proportion (1 NHBE cell: 1 macrophage). MDM were also used in cultures stimulated with recombinant human IL-6.

AEC kinetic and co-culture

For kinetic experiments, Calu-3 were infected with SARS-CoV-2 at an MOI of 0.2 or 2.0 for 6, 12, 24, 48, 72, 96, 120 and 144 h at 37°C and 5% CO_2. Viral load and inflammatory mediators were assessed in supernatants, protein was evaluated in lysate cells and the type of cell death was evaluated in detached cells after treatment with trypsin (Gibco). For treatment experiment, approximately $5x10^5$ Calu-3 cells were pre-treated with kp7-6 (100 μg/mL, CD95/CD95L antagonist, Sigma-Aldrich)[49] for 2 h and then infected with SARS-CoV-2 at an MOI of 0.2. For co-culture experiments, Calu-3 were infected with SARS-CoV-2 at an MOI of 0.2 for 72 h and detached cells were stained with FVS and annexin V.

Apoptotic cells (annexin V^+) were freshly sorted in FACS Melody (BD Biosciences, San Jose, CA) allocated in a biosecurity level 3 laboratory (Department of Biochemistry and Immunology, Ribeirao Preto Medical School, University of Sao Paulo, Ribeirao Preto, Sao Paulo, Brazil). Sorted AEC were then co-cultured with TDM for 24 h in an equal proportion (1 apoptotic cell: 1 macrophage).

Macrophage stimulation and treatments

Approximately 2.5×10^5 TDM were stimulated with a pool of cell-free supernatants derived from TA samples of COVID-19 patients in an equal proportion with culture medium (1:1 v/v) for 24 h at 37°C and 5% CO_2. Approximately 2.5×10^5 TDM and MDM were stimulated with recombinant human IL-6 (200, 2,000 or 4,000 pg/mL, PeproTech) for 24 h at 37°C and 5% CO_2. Approximately 2.5×10^5 TDM cells were pre-treated with tocilizumab (100 μg/mL, Actemra) for 1 h and then stimulated with recombinant human IL-6. Approximately 5×10^5 MDM were pre-treated with kp7-6 (100 μg/mL) for 2 h and pre-treated with tocilizumab (100 μg/mL) for 1 h and then stimulated with recombinant human IL-6. Inflammatory mediators were assessed in supernatants and protein expression was analyzed using flow cytometry in detached cells after treatment with EDTA (5 mM).

Mice infection and sample collection

Mice were infected with 5×10^5 PFU of WT SARS-CoV-2 variants by intranasal route. Mice were euthanized 3 days post infection and the lungs were collected for analysis. The superior right lobe was gently perfused with 10% formaldehyde solution, embedded in paraffin, sectioned at 4 μm thickness and stained with Harris's hematoxylin and eosin (H&E) for histopathological analysis. Pulmonary inflammation score was determined as degree: 0 (without inflammation) - absence or presence of rare inflammatory cells; 1 (mild inflammation) – mild perivascular or peribronchial accumulation of inflammatory cells; 2 (moderate inflammation) - perivascular or peribronchial accumulation of inflammatory cells, sometimes coalescing and preserving alveolar spaces; 3 (severe inflammation) - perivascular or peribronchial accumulation of inflammatory cells, mostly coalescing and preserving rare alveolar spaces. The left lung was collected in complete RPMI media and processed for flow cytometry analysis. The middle and inferior right lobes were weighted and homogenized with PBS (1:5 w/v) using a 5 mm stainless steel bead (Qiagen, USA) and a TissueLyser LT (Qiagen, USA), (50 Hz for 5 min), centrifuged at 10,000 x g for 10 min, and the supernatant was collected and used for viral load measurement by plaque assay and qRT-PCR and cytokines quantification.

Soluble immune mediators

IL-1β, IL-6, IL-10, and TNF levels were determined in the supernatants of Calu-3 and macrophage cultures using ELISA kits following the manufacturer's instructions (R&D Systems). HMGB-1 was determined in the cell-free TA supernatants and in the supernatants of Calu-3 cultures using immunoassay following the manufacturer's instructions (Novus Biologicals). Adenosine 5′-triphosphate (ATP) was assessed in the cell-free TA supernatants using bioluminescent assay kit following the manufacturer's instructions (Sigma-Aldrich). The levels of soluble immune mediators were measured in TA samples using a high-throughput microbeads array (Bio-Plex Pro Human Cytokine 27-plex Assay, Bio-Rad Laboratories, Hercules, CA, USA), following the manufacturer's instructions. The results were expressed in pg/mL according to standard curves for each immune mediator using a fifth parameter logistic fit analysis. Cytokine profile in the lung of infected mice was determined using the Cytometric Bead Array (CBA) Mouse Th1/Th2/Th17 Cytokine kit (BD Biosciences) according to manufacturer instructions and samples were acquired on BD FACSCanto (BD Biosciences, USA) and analyzed using FCAP Array v3.0 (BD Biosciences, USA).

Flow cytometry

Calu-3 and NHBE were detached with trypsin (Lonza) and TDM or MDM were detached with EDTA (5 nM); all cells were washed with PBS, incubated with Fixable Viability Stain (FVS, BD Bioscience) and washed with PBS-1% FBS. AEC cells were stained with CD95 PerCP eFluor-710 (APO-1/Fas, clone DX2) and CD178 APC (CD95L, Fas-ligand, clone NOK-1) and washed with biding buffer for annexin V PE-Cy7 stain (Thermo Scientific) and macrophages were stained with HLA-DR PE-Cy7 (clone LN3), CD163 PE (clone GHI/61), CD95 PerCP eFluor-710 (APO-1/Fas, clone DX2) and CD178 APC (CD95L, Fas-ligand, clone NOK-1). Freshly or frozen cells isolated from TA of COVID-19 patients were washed with PBS, incubated with FVS (BD Bioscience) and washed with PBS-1% FBS. Cells from TA were then stained with CD45 PE-Cy7 (clone 2D1), EpCAM PE (clone EBA-1), CD95 PerCP eFluor-710 (APO-1/Fas, clone DX2) and CD178 APC (CD95L, Fas-ligand, clone NOK-1). Lung cells from mice were isolated by proper right lung lobules digestion using collagenase (2.2 mg/mL, Sigma-Aldrich) and DNAse (0.055 mg/mL, Roche). Samples were incubated with Live/Dead viability stain (Thermo Scientific), purified anti-mouse CD16/CD32 (Fcγ III/II receptor, clone 2.4G2) and then stained with CD45 PE-Cy7 (clone 30-F11), CD31 PE-Cy7 (clone 390) and CD326 BB515 (EpCAM, clone G8.8) for AEC or stained with CD11b BV711 (clone M1/70), CD11c PE-Cy7 (clone HL3), SiglecF BB515 (clone E50-2440) and MHCII BB700 (IA/IE, clone M5/114.15.2) for macrophages, according to antibodies fabricant instructions (BD Pharmingen and eBioscience). Samples with annexin V were freshly acquired in FACS Melody (BD Biosciences) and others were fixed using PBS containing 1% paraformaldehyde (Labsynth, Diadema, SP, Brazil) and acquired in FACS Canto II (BD Biosciences). Analyses were performed in FlowJo software (Becton Dickinson and Company).

Western blot

Calu-3 were lysed with RIPA buffer (150 mM NaCl, 5 mM EDTA, 50 mM TRIS, 1%

NP-40, 0.5% sodium deoxycholate, 0.1% SDS) supplemented with a protease inhibitor cocktail (Sigma) and clarified and boiled in Laemmli's buffer. Samples were resolved by SDS-PAGE in a 10% polyacrylamide gel, transferred to 0.20 μm nitrocellulose membrane (BIO-RAD) and blocked with 5% nonfat dry milk for 1 h. Proteins were detected using rabbit anti-cleaved caspase 3 (1:250, Cell Signaling) or rabbit anti-cleaved caspase 8 (1:250, Cell Signaling) and HRP-conjugated anti-rabbit anti-β actin (1:10000, Cell Signaling). Chemiluminescence was detected with Clarity Western ECL substrate (Bio-RAD) and imaged with a ChemiDOC Imaging System (Bio-RAD).

QUANTIFICATION AND STATISTICAL ANALYSIS

Transcriptome analysis

The transcript expression data was obtained from public data deposited at *Gene Expression Omnibus* database.[50] We selected count raw data for the transcript reads for independent biological triplicates for SARS-CoV-2 (USA-WA1/2020 strain) infected and mock Calu-3 deposited by Blanco-Melo et al.[8] with id GSE147507. Differential gene expression analysis of SARS-CoV-2 infected versus mock control was carried out using with *DESeq2*. The p values derived from differential expression analysis were adjusted (p_{adj}) for multiple testing using the Benjamini and Hochberg method.[51] Differentially expressed gene (DEG) signature was defined using a threshold for absolute value of fold-change at $\log_2$ basis >0.5 and $p_{adj} < 0.05$. The DEG list was submitted to over-representation analysis using *cluster Profiler* over *Reactome pathways* annotations within BH adjusted p value <0.05. The heatmap for normalized gene expression was constructed using *pheatmap*. The data was analyzed in *R* environment (https://www.R-project.org/).

Statistical analysis and figures

Data were analyzed using GraphPad Prism Version 8.1 (GraphPad Software, Inc., San Diego, CA, USA). Normality of data was analyzed by Shapiro-Wilk test. The comparison between two groups was performed using t-test or Mann-Whitney test. Comparisons among three groups were performed using one-way ANOVA followed by Tukey's test or Kruskal-Wallis test. The histological score was calculated by the Chi-square test. Data were shown as the mean ± standard deviation (SD) in case of normality or shown as box with min-to-max in case of asymmetric distribution. The results were considered significant with a p value less than 0.05. Graphics were made in GraphPad Prism and figures were made using free images from Servier Medical Art (https://smart.servier.com/). Spearman's correlation matrix was constructed using R base functions and *qgraph* was used to build the network illustration for pair correlations.